

A New Type of DNA Minor-Groove Complex: Carbazole Dication–DNA Interactions[†]

Fariat A. Tanious,[‡] Daoyuan Ding,[‡] Donald A. Patrick,[§] Richard R. Tidwell,[§] and W. David Wilson^{*,‡}

Department of Chemistry and Laboratory for Chemical and Biological Sciences, Georgia State University, Atlanta, Georgia 30303, and Department of Pathology, University of North Carolina, Chapel Hill, North Carolina 27599

Received July 2, 1997; Revised Manuscript Received September 22, 1997[⊗]

ABSTRACT: The effect of opportunistic infections (OI) on immune-compromised populations has been known for decades, but the recent AIDS epidemic has sparked renewed interest in the development of new anti-OI agents. The mechanism of action of a series of cationic unfused-aromatic anti-OI drugs is believed to involve binding of the drug to AT sequences in the minor groove of DNA. Some new anti-OI drug candidates have been synthesized with fused aromatic ring systems (e.g. carbazoles) that do not resemble the classical paradigm for minor-groove interactions at AT sequences in DNA. To characterize the DNA interactions of these compounds, we have used UV–vis absorbance, fluorescence, kinetic measurements, and circular dichroism in conjunction with NMR spectroscopy to evaluate the structure of the complexes formed between the carbazoles and DNA. Application of these methods to carbazoles substituted at either the 3,6 or 2,7 positions with cationic imidazoline groups gave conclusive, but very surprising, evidence that both compounds bind strongly in the minor groove at AT DNA sequences. NMR and molecular modeling of the complexes formed between the 3,6- and 2,7-carbazoles and the self-complementary oligomer d(GCGAATTCGC) have been used to establish structural details for the minor-groove complex. These results have been used as constraints for molecular modeling calculations to construct models of the minor-groove–carbazole complexes and to draw conclusions regarding the molecular basis for the effects of substituent position on carbazole–DNA affinities. The surprising result is that the 2,7 carbazole binds in AT sequences with hydrogen bonds involving one imidazoline group and the carbazole NH. The 3,6-carbazole compound binds in a more “classical” model that uses both imidazoline groups for H-bonding while the carbazole NH points out of the minor groove. The carbazoles thus form a new type of DNA minor groove complex and their excellent biological activities indicate that a variety of fused-ring minor-groove binding agents should be investigated.

Organic cations that bind in the minor groove of DNA typically have extended conjugated systems with unfused aromatic rings that are directly bonded (such as DAPI, Hoechst 33258, furamidine) or are connected through conjugated systems (such as netropsin, distamycin, berenil, and stilbamidine) (1–10). Pentamidine, which is being used clinically against *Pneumocystis carinii pneumonia* (PCP), a leading cause of morbidity and mortality in AIDS patients, (11, 12) is a related type of structure with the aromatic groups linked through an alkyl chain. The mechanism of action of pentamidine and derivatives is believed to involve formation of a complex with the DNA of the microorganism, followed by selective inhibition of a DNA interactive microbial enzyme. There is now considerable evidence that in some cases the enzyme inhibited by the pentamidine–DNA complex is topoisomerase II of the organism (13–15) and this inhibition rapidly leads to cell death.

Pentamidine binds in the DNA minor groove in AT sequences (16, 17) and shows some side effects that limit its drug use (13). We are involved in the design, synthesis, and study of new minor-groove binding cations with the goal

of improving efficacy by enhancing specific DNA binding interactions and microbial enzyme inhibition selectivity (18–20).

As part of our extended investigation to develop new anti-opportunistic infections (OI) drugs and examine their interaction with DNA, we have investigated the binding mode of new 2,7- and 3,6-carbazole dications to AT and GC rich sequences of DNA. Interestingly, these derivatives exhibit some of the best anti-*Pneumocystis* activity yet seen in the dication series (21). On the basis of kinetic and spectroscopic, particularly NMR, results, we report here the surprising finding that both of these fused aromatic cations bind in the minor groove in AT sequences. Such compounds could in principle bind to AT sequences by intercalation, but the minor-groove interactions in AT sequences are favorable, and the binding energy minimum is for a minor groove rather than an intercalation complex. We present molecular models to demonstrate that the carbazoles, particularly the 2,7 substituted compound, form new types of minor-groove complexes in AT sequences of DNA.

MATERIALS AND METHODS

The carbazoles were prepared as reported previously (21). Purity of all compounds was verified by NMR and elemental analysis.

Buffer. MES buffer contained 0.01 M MES and 1×10^{-3} M EDTA. Sodium chloride was added to adjust the ionic

[†] This work was supported by NIH Grant AI-33363. Instrumentation was purchased through funds from the Georgia Research Alliance.

* Corresponding author. Tel: 404-651-3903. Fax: 404-651-2751. E-mail: chewdw@panther.gsu.edu.

[‡] Georgia State University.

[§] University of North Carolina.

[⊗] Abstract published in *Advance ACS Abstracts*, November 15, 1997.

strength, and the pH was adjusted to 6.2 with NaOH. Phosphate buffer contained 7.5 mM sodium phosphate, 100 mM NaCl, and 0.01 mM EDTA, pH 7.0.

DNA. The polymers poly[d(G-C)]₂ and poly[d(A-T)]₂ (Pharmacia) were prepared as previously described (22). The oligomers d(G-C)₇, d(A-T)₇, and d(GCGAATTCGC) (Midland Certified Reagent Co.) and were purified by HPLC and desalted. The concentrations were determined optically using extinction coefficients per mole of strand at 260 nm determined by the nearest neighbor procedure (23).

Absorption Spectroscopy. UV-vis scans were obtained as previously described (24, 25) with a Cary 4 spectrophotometer in MES with 0.1 M NaCl added. Spectrophotometric binding measurements have been described (25).

Fluorescence Spectroscopy. Fluorescence spectra were obtained on a Photon Technology International (PTI) spectrometer with Felix software, which controls the instrument and collects the fluorescence data. Typically, fluorescence intensity for the compound was measured at 20 °C in MES buffer, the samples were excited at 320 nm, and the fluorescence emission was monitored. The solution of the compound was titrated with aliquots of DNA stock solution. The following equation was used to calculate C_b , the concentration of bound compound:

$$C_b = (I_0 - I_i) / [(1 - I_b/I_0)(I_0/C_0)] \quad (1)$$

where I_0 is the initial fluorescence intensity, I_i is the fluorescence intensity at each concentration of DNA, I_b is the fluorescence intensity at saturation, and C_0 is the initial concentration of the compound. The concentration of the free compound and the Scatchard parameters can be obtained from

$$C_{\text{free}} = C_0 - C_b \quad (2)$$

Circular Dichroism. CD spectra were obtained on a computer-controlled Jasco J-710 spectrometer with the software supplied by Jasco for instrument control and data acquisition. Solutions of the compounds in MES buffer at 25 °C were scanned in 1 cm quartz cuvettes. A solution of the DNA was scanned, the compound was then added, and the sample was rescanned at all desired ratios.

DNA Thermal Melting. Thermal melting experiments were conducted with Cary 3 or Cary 4 spectrophotometers interfaced to microcomputers as previously described (26). A thermistor fixed into a reference cuvette was used to monitor the temperature. The DNA or oligomer was added to 1 mL of buffer (MES with 0.1 M NaCl added) in 1 cm path length reduced volume quartz cells, and the concentration was determined by measuring the absorbance at 260 nm. Experiments were generally conducted at a concentration of 5×10^{-5} M base pairs for the polydA·polydT and 3×10^{-6} M in duplex for d(CGCGAATTCGCG)₂. For the complex T_m experiments a ratio of 0.6 compound per base pair for polydA·polydT and a ratio of 1 compound per oligomer duplex for d(CGCGAATTCGCG)₂ were used.

Kinetics. Kinetics experiments were conducted on an Olis RSM 1000 scanning stopped-flow spectrometer interfaced to Gateway 2000 PC computer. Global analysis is provided with the RSM-1000 software, and single wavelength fitting can be performed at any selected wavelength.

NMR Spectra of the Carbazoles with d(A-T)₇ and with d(G-C)₇. NMR spectra were obtained on a Varian Unity plus 600 spectrometer as previously described (9, 27). Data were processed either by Vnmr 5.1 software from Varian or with the program FELIX (Biosym Technologies, San Diego, CA). Typical conditions for the collection of spectra in D₂O included 6000 Hz spectral width, 2000 scans, 1-s relaxation delay, 0.6 mL of sample in a 5 mm NMR tube, and 1.5 Hz line broadening before Fourier transformation. A relatively low concentration of drug (0.2 mM) was necessary both to prevent precipitation of the complexes and to insure that no concentration induced shifts of the free drug were observed. Titrations were conducted over a range of drug-DNA ratios from 2.5 to 0.2 under fast exchange conditions (temperature > 35 °C). Temperature studies were conducted from 25 to 85 °C. Spectral lines were very broad below 20 °C. All NMR spectra were obtained in phosphate buffer solution (7.5 mM NaH₂PO₄, 10⁻⁵ M EDTA, pH 7.0, 0.10 M NaCl). Samples were referenced to DSS using the calibrated position of the water peak relative to DSS. Assignment of the aromatic proton signals for the drug-DNA complexes were made via drug-DNA titrations, melting 1D, or 2D COSY experiments.

NMR Spectra of the Carbazoles with d(CGCGAATTCGCG)₂. The carbazoles were dissolved in 99.96% D₂O (Isotec). For the 1:1 ratio of DNA duplex to ligand, 1 mmol of the carbazole was added to 1 mmol of the DNA duplex solution in the NMR tube. The solvent was removed under N₂ and 0.6 mL of 99.996% D₂O added, solvent removed, and the sample rehydrated with 0.6 mL of 99.996% D₂O. All of the 1D and 2D ¹H spectra were collected on Varian Unity plus 500 or 600 MHz spectrometers and the data transferred to a Silicon Graphics workstation for processing with FELIX. One-dimensional experiments were obtained with a spectral width of 4500 Hz, 16000 complex data points, a 1-s relaxation delay, and 100–500 transients. The residual HDO peak was used as an internal reference. Two-dimensional experiments were obtained with a spectral width of 6000 Hz in both dimensions with 2048 complex data points in the t_2 dimension and 512 points in the t_1 dimension. Phase sensitive NOESY spectra were obtained with a mixing time of 300 ms by using the method of States (28).

Molecular Mechanics and Modeling. All models were built and energy minimized using the software package Sybyl (v6.03, Tripos). The Kollman all-atom forcefield (29, 30) was used with minor modifications as described previously (31). The X-ray coordinates of the furan complex with d(CGCGAATTCGCG)₂ (32) from the Brookhaven Protein Databank (PDB file 227D) were used as a starting point for docking the carbazole into the DNA structure. The ends of this dodecamer were capped with 5' and 3' OH groups. The carbazoles were built in Sybyl and the geometry optimized using MNDO charges. The compounds were then visually docked into the diphenylfuran binding site of the DNA, and the furan was deleted. The initial docking with the compounds used the position of the diphenylfuran from the X-ray structure and the NOE interactions as guides. As the final docking was in progress, hydrogen bonding between the carbazole and AT base pairs at the floor of the minor groove were optimized. For the initial geometry optimization of this complex the DNA was treated as an aggregate in Sybyl and the NMR crosspeaks between the ligand and DNA were

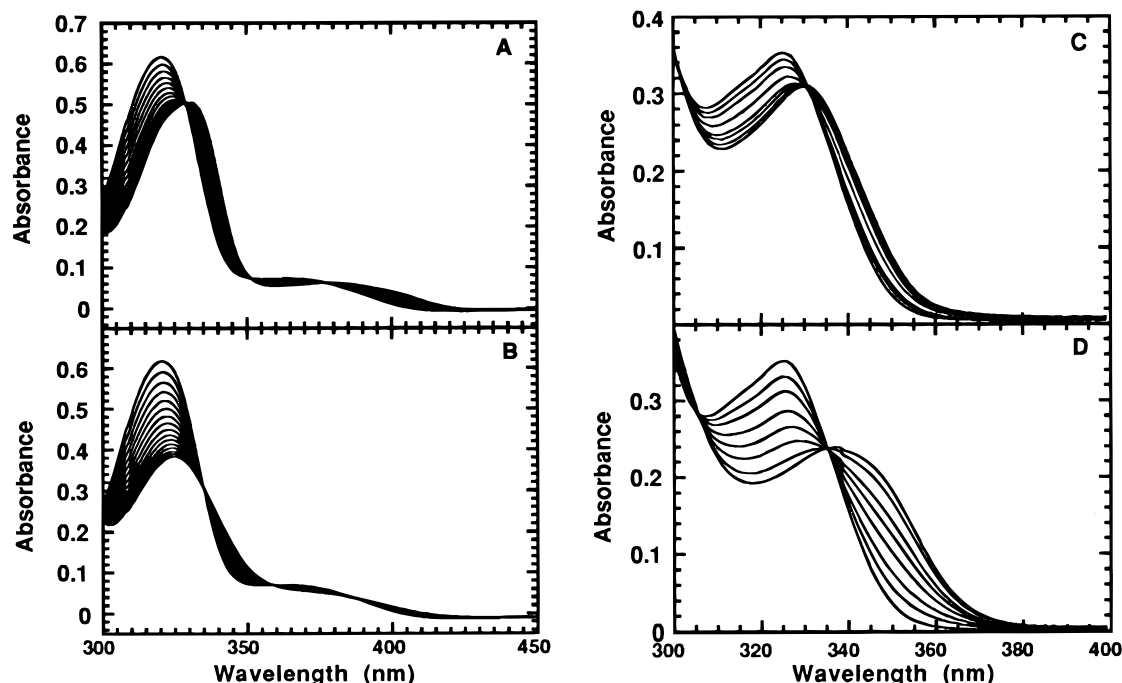


FIGURE 1: Spectrophotometric titrations of the 2,7-carbazole (A, B), and the 3,6-carbazole (C, D) with poly[d(A-T)]₂ and poly[d(G-C)]₂. Titrations were conducted in a 1 cm cell in MES buffer with 0.1 M NaCl added at 25 °C. (A) The concentrations are as follows: 1.86×10^{-5} M of 2,7-carbazole, and poly[d(A-T)]₂ concentrations in base pairs of zero, 5.35×10^{-6} , 1.07×10^{-5} , 1.6×10^{-5} , 2.13×10^{-5} , 2.65×10^{-5} , 3.18×10^{-5} , 3.7×10^{-5} , 4.22×10^{-5} , 4.74×10^{-5} , 5.25×10^{-5} , 5.75×10^{-5} , 6.30×10^{-5} , 6.8×10^{-5} , and 7.30×10^{-5} respectively from the top to the bottom curves at 320 nm. (B) The concentrations are as follows: 1.86×10^{-5} M of 2,7-carbazole, and poly[d(G-C)]₂ concentrations in base pairs of zero, 5.35×10^{-6} , 1.07×10^{-5} , 1.6×10^{-5} , 2.13×10^{-5} , 2.65×10^{-5} , 3.18×10^{-5} , 3.7×10^{-5} , 4.22×10^{-5} , 4.74×10^{-5} , 5.25×10^{-5} , 5.75×10^{-5} , 6.30×10^{-5} , 6.8×10^{-5} , 7.30×10^{-5} , and 7.8×10^{-5} respectively from the top to the bottom curves at 320 nm. (C) The concentrations are as follows: 1.86×10^{-5} M of 3,6-carbazole, and poly[d(A-T)]₂ concentrations in base pairs of zero, 5.35×10^{-6} , 1.07×10^{-5} , 2.24×10^{-5} , 3.5×10^{-5} , 4.36×10^{-5} , 6.06×10^{-5} , and 8.56×10^{-5} respectively from the top to the bottom curves at 325 nm. (D) The concentrations are as follows: 1.86×10^{-5} M of 3,6-carbazole, and poly[d(G-C)]₂ concentrations in base pairs of zero, 5.35×10^{-6} , 1.07×10^{-5} , 2.24×10^{-5} , 3.5×10^{-5} , 4.36×10^{-5} , 6.06×10^{-5} , and 8.56×10^{-5} respectively from the top to the bottom curves at 325 nm.

used as range constraints ($2\text{--}4 \text{ \AA}$, $25 \text{ kcal}/(\text{mol} \cdot \text{\AA}^2)$ force constant). Hydrogen-bonding constraints were included with a distance of 3 \AA between the heavy atoms with initial constraints constant of $25 \text{ kcal}/(\text{mole} \cdot \text{\AA}^2)$. The complexes were then energy minimized to a rms gradient of $0.08 \text{ kcal}/(\text{mol} \cdot \text{\AA})$ using the Powell method. The aggregate on the DNA was removed, and the complex energy was minimized to a rms gradient of $0.08 \text{ kcal}/(\text{mol} \cdot \text{\AA})$. Finally, the constraints were removed and the complex energy minimized to a rms gradient of $0.08 \text{ kcal}/(\text{mol} \cdot \text{\AA})$ in SYBYL.

RESULTS

Spectral Changes on Complex Formation. (a) *UV–Visible Absorption Spectral Changes.* Both poly[d(A-T)]₂ and poly[d(G-C)]₂ induce significant shifts in the UV–vis spectra of the fused heterocyclic carbazole compounds. The shifts induced by the two polymers are, however, quite different (Figure 1). Addition of poly[d(A-T)]₂ to both compounds results in shifts of the spectrum to longer wavelength and an approximately 20–25% decrease in extinction coefficient at the peak wavelength (Figures 1A and 1C). With poly[d(G-C)]₂ there is less shift to longer wavelength with the 2,7 carbazole, but there is a 40% decrease in extinction coefficient. Addition of poly[d(G-C)]₂ to the 3,6 carbazole results in significant shifts of the spectrum to longer wavelength, a large decrease in extinction coefficient, and a broadening of the carbazole spectral band (Figure 1D). Clearly there are strong interactions of the carbazole aromatic systems with AT and GC base pairs for both the 2,7 and 3,6

compounds, but the interaction are sufficiently varied to induce quite different perturbations in the carbazole system.

(b) *Fluorescence Spectral Changes.* Fluorescence titrations of the 2,7 and 3,6 carbazole derivatives with poly[d(A-T)]₂ and poly[d(G-C)]₂ are shown in Figure 2. The free 2,7 carbazole has a strong fluorescence emission at 440 nm. Addition of poly[d(A-T)]₂ cause an approximately 40% increase in the fluorescence (Figure 2A). Addition of poly[d(G-C)]₂ causes a very slight shift of the peak maximum to longer wavelength and causes a large decrease in fluorescence intensity (Figure 2B).

The free 3,6-carbazole has a strong fluorescence emission at 415 nm. Addition of poly[d(A-T)]₂ causes a significant shift of the peak maximum to lower wavelength and causes an approximately 40% decrease in the fluorescence at the 415 nm peak (Figure 2C). Addition of poly[d(G-C)]₂ to the 3,6 carbazole causes a large decrease in fluorescence intensity with little shift in peak wavelength (Figure 2D), similar to the effects with the 2,7 derivative.

(c) *Circular Dichroism (CD).* CD spectra were obtained for carbazole complexes in both the wavelength region above 300 nm, where DNA does not absorb and all bands are due to induced CD in the bound carbazoles, and in the region below 300 nm where both DNA and the compounds absorb (Figures 3A–D). In contrast to absorption spectral results, CD changes are much larger for complexes with the AT than with the GC polymer. Addition of the 2,7 carbazole to poly[d(A-T)]₂ in 0.1 M NaCl results in an increase of the signal at 260 nm, a decrease at 280 nm, and small increase at 230

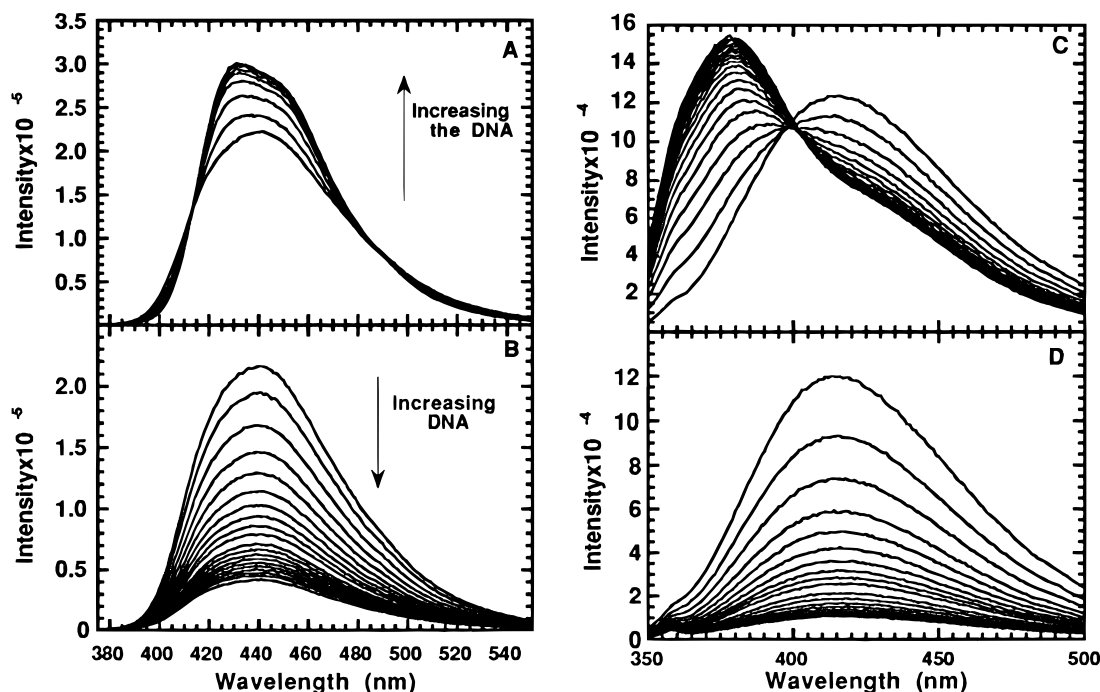


FIGURE 2: Fluorescence emission spectral titrations of the 2,7-carbazole (A, B), and the 3,6-carbazole (C, D) with poly[d(A-T)]₂ and poly[d(G-C)]₂. Titrations were conducted in a 1 cm cell with a concentration of 1×10^{-6} M of the compound in MES buffer with 0.1 M NaCl added at 25 °C. The excitation wavelength for both compounds was 320 nm, the excitation slit was at 1 nm, and the emission slit at 4 nm.

nm. In the drug region, strong positive CD signals at 295 and 335 nm are induced. Very clear isoelliptic points at 235, 260, 270, and 290 nm (Figure 3A) are observed. Addition of the 2,7 carbazole to poly[d(G-C)]₂ results in a very small induced CD signal in the drug spectrum but does cause a CD increase between 260 and 280 nm (Figure 3B).

Addition of the 3,6-carbazole to poly[d(A-T)]₂ results in a CD decrease in the DNA region at 260 nm and a small increase at 230 nm. There are strong positive induced CD signals at 294 and 335 nm with very clear isoelliptic points at 280 and 240 nm (Figure 3C). Addition of poly[d(G-C)]₂ to the 3,6-carbazole results in a weak positive CD signal at 340 nm and an increase in the DNA region from 260 to 280 nm (Figure 3D). Results with the GC polymer are quite similar for the two complexes below 300 nm, as are the induced CD spectra above 300 nm for the AT polymer complexes. As with the absorption and fluorescence spectral results, the CD results illustrate that both carbazoles have strong but quite distinct complexes at AT and GC base pair sequences.

(d) *NMR*. To evaluate binding differences in AT and GC base pair sequences, NMR spectral titrations of the carbazoles were carried out with oligomer duplexes d(A-T)₇ and d(G-C)₇ as a function of temperature (Figure 4). Carbazole proton assignments in the complexes were made by monitoring chemical shift changes on titration of the compounds with DNA, and by collecting 2D COSY and NOESY spectra for the complexes. COSY spectra were sufficient to identify the carbazole aromatic protons in the compound–DNA complexes (a 2D COSY spectrum for the 2,7 carbazole complex is shown in the Supporting Information, Figures S1A and B). The studies are concentrated on the aromatic proton region for both drug and DNA resonances as this region is most sensitive to the compound–DNA binding mode (33). GC and AT base pairs are both characterized by purine H8 and pyrimidine H6 signals in the aromatic

region while AT base pairs have an additional AH2 proton resonance. These signals are quite broad at low temperature but become sharper as the temperature approaches the T_m. The carbazoles are symmetric compounds and have only three CH aromatic proton NMR signals in solution (Figure 4). When bound to DNA, however, it is possible that the two sets of protons on opposite sides of the carbazole ring system could be in different environment with different chemical shifts. At high temperature only a single set of signals is seen, suggesting fast exchange of the carbazole such that differences in environment for the two sides of the carbazole are averaged. At low temperature the signals become significantly broadened, indicating an intermediate exchange region.

The drug aromatic proton signals are well resolved, and upon addition of d(G-C)₇ or d(A-T)₇ display one of two distinct types of behavior: the carbazole proton signals for both the 2,7 and 3,6 substituted compounds are shifted significantly upfield from 0.45 to 0.75 ppm at all ratios upon addition of d(G-C)₇ (Figure 4B and Table 1), while addition of d(A-T)₇ causes small, upfield and downfield chemical shift changes (Figure 4A and Table 1). These changes of the aromatic proton chemical shifts for d(A-T)₇ complexes indicate that the compound protons are not being influenced by major ring current effects as would be expected for an intercalation binding mode. The carbazole signals in the AT complex move upfield on heating, indicating that the carbazoles begin to stack with the bases as the DNA is denatured and the minor groove of the duplex is lost on denaturation. Very different behavior is obtained on heating the GC complex. The carbazole signals move downfield as the DNA is denatured, indicating a weaker stacking with bases in denatured than in the native GC oligomer.

To obtain additional structural information on the carbazole–AT complexes, NMR spectra of the compounds complexed with d(GCGAATTCGC)₂ at a 1:1 ratio were

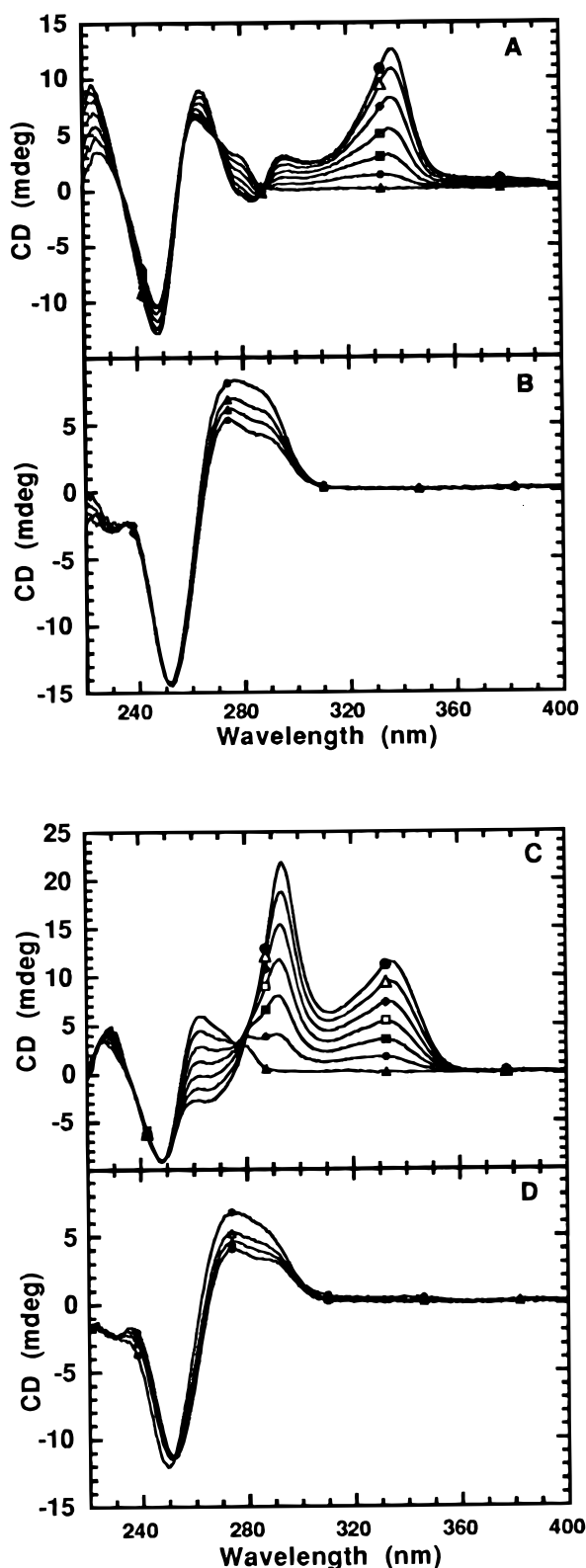


FIGURE 3: CD spectra of the carbazole compounds, (A) the 2,7 with poly[d(A-T)]₂, (B) the 2,7 with poly[d(G-C)]₂, (C) the 3,6 with poly[d(A-T)]₂, and (D) the 3,6 with poly[d(G-C)]₂. Experiments were conducted in a 1 cm cell in MES buffer with 0.1 M NaCl added at 25 °C at a polymer concentration of 2.32×10^{-5} M in base pairs. The ratio of compound/poly[d(A-T)]₂ in base pairs is 0 (▲), 0.05 (○), 0.10 (■), 0.15 (□), 0.20 (◆), 0.25 (△), and 0.3 (●). The ratio of compound/poly[d(G-C)]₂ in base pairs is 0 (●), 0.05 (▲), 0.10 (△), and 0.20 (○).

obtained. Proton chemical shifts were assigned through a combination of 1D titration spectra, as well as 2D NOESY, and COSY experiments. For the free DNA, the chemical

shift assignments of the nonexchangeable protons have been confirmed (34–36). Spectra for the 2,7-carbazole are shown in Figure 5 for illustration: plots of the aromatic region of the free drug, free d(GCGAATTCGC)₂, and the NMR spectra for the 1:1 complex at 25–45 °C are shown. Below 25 °C substantial line broadening occurs (not shown). At 35 °C and above the signals are sharper as the complex moves to fast exchange. In the 1D spectra (Figure 5) major downfield shifts are seen for A5-H2 and the aromatic protons of the carbazole while the T6-H6 protons in the major groove shift upfield. The change in chemical shifts upon binding the ligand for several proton signals along the duplex are plotted in Figure 6, and it can be seen that the most dramatic changes occur in the central AT rich region.

The aromatic to H1' region of the 2D NOESY spectrum for the 1:1 complex of the 2,7 carbazole with d(GCGAATTCGC)₂ at 35 °C is shown in Supporting Information, Figure S2, for illustration of assignment results with both carbazoles. Figure 7 shows one of the strong crosspeaks between the carbazole (H1/H8) and DNA (A5-H2) and two weaker crosspeaks, H1/H8 to A5-H1' and H1/H8 to T6-H1'. This observation confirms a minor-groove binding mode in the central AT region of this duplex for the carbazole and defines the carbazole orientation in the complex.

The 2D NOESY spectrum for the 1:1 complex of the 3,6-carbazole with d(GCGAATTCGC)₂ at 35 °C (not shown) has a strong crosspeak between the ligand (H4/H5) and DNA (A5-H2) as well as a weaker crosspeak from H4/H8 to T6-H1'. This observation also confirms a minor-groove binding mode in the central AT region of this duplex for the 3,6-carbazole and fixes the carbazole orientation in the groove. These results clearly illustrate that the 2,7- and 3,6-carbazoles fit into the DNA minor groove in opposite orientations with respect to the carbazole NH group.

Binding Kinetics. Spectral changes (for example, Figure 1) observed on binding of the carbazoles to poly[d(A-T)]₂ and poly[d(G-C)]₂ polymers were used to monitor the kinetics of binding. A plot of absorbance spectral changes as a function of time for dissociation of the 2,7-carbazole from poly[d(A-T)]₂ is shown in Figure 8 for illustration. Two exponential fits to the data are also shown along with plots of residuals. Single-exponential fits generally give unsatisfactory residuals and significantly higher rms deviations with all the complexes of these compounds with poly[d(A-T)]₂ and poly[d(G-C)]₂. Two exponential fits to the data give satisfactory residuals, and three exponential fits do not significantly improve the residuals or rms deviations.

For the purposes of comparison, the dissociation lifetime (τ) and apparent rate constant ($k_{\text{app}} = 1/\tau$) were calculated from the computer-derived, best-fit values for rate constants and amplitudes:

$$\tau = 1/(A_1k_1 + A_2k_2) \quad (3)$$

where A and k values refer to the amplitudes and rate constants for the two exponential fits to the dissociation results. Dissociation rate constants were measured as a function of salt concentration at constant temperature, and linear plots of $\log(k_{\text{app}})$ as a function of $-\log[\text{Na}^+]$ are shown in (Supporting Information, Figure S3). For the SDS driven dissociation of the two compounds from poly[d(G-C)]₂, a slope of 0.7 ± 0.1 is obtained, similar to the slope for the dicationic intercalator propidium (25). A quite different

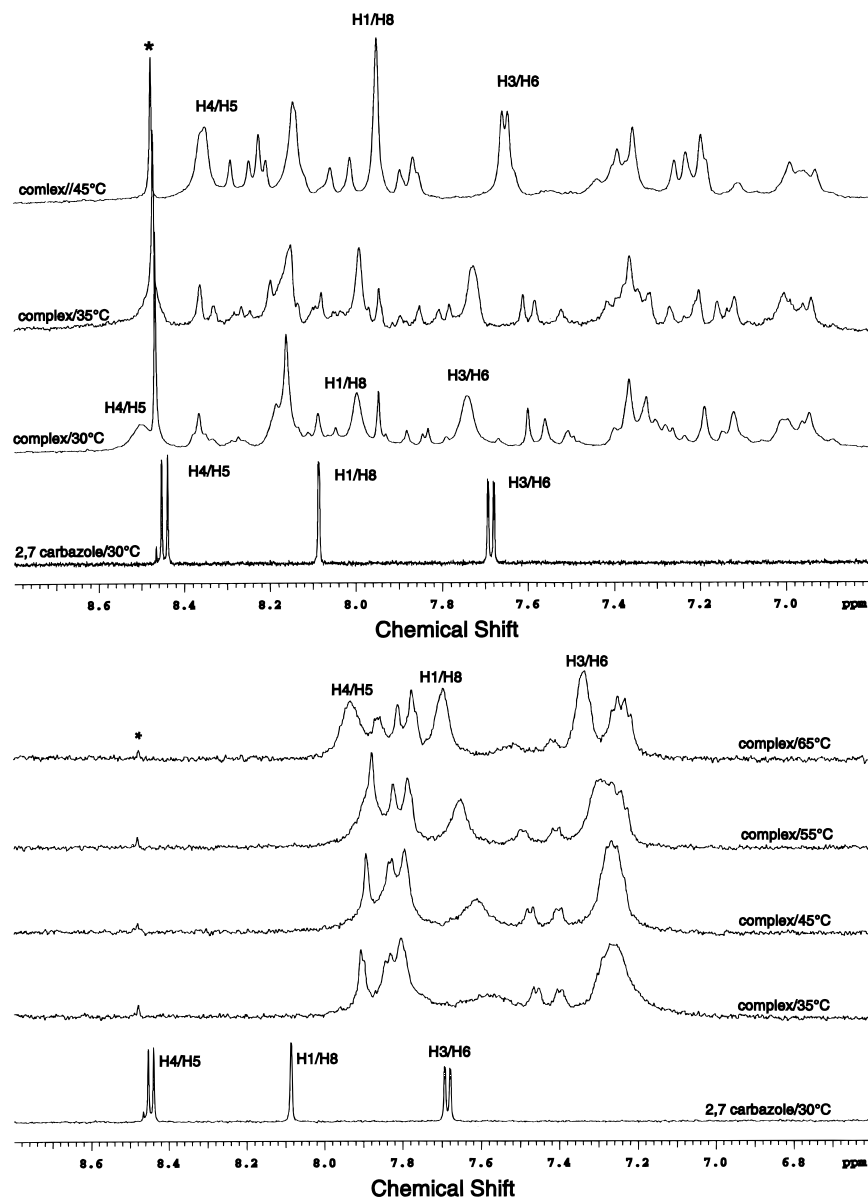


FIGURE 4: (A, top) Proton NMR spectra of the aromatic region of the 2,7-carbazole with the oligomer d(A-T)₇. The concentration of the compound was 0.2 mM, and the ratio of the compound to DNA base pairs was 0.3. The peak labeled with asterisk is impurity from D₂O. (B, bottom) Proton NMR spectra of the aromatic region of the 2,7-carbazole with the oligomer d(G-C)₇. The concentration of the compound was 0.2 mM, and the ratio of the compound to DNA base pairs was 0.5. The peak labeled with asterisk is impurity from D₂O.

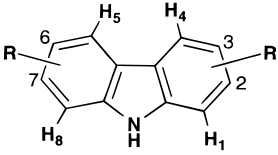
slope of 1.7 ± 0.1 is obtained with poly[d(A-T)]₂, similar to the slope obtained for minor-groove binding compounds with poly[d(A-T)]₂ (9, 37–39).

The association reaction of the 3,6-carbazole with poly[d(A-T)]₂ as an example was also followed by stopped-flow methods. The association results are plotted in (Supporting Information, Figure S4) as a function of salt concentration. Results for DAPI which binds in the minor groove in AT sequences, the dicationic intercalator propidium, and a naphthalene diimide which binds by a threading intercalation mode are included in the figure for reference. As with the dicationic diamidine DAPI, the carbazole binds to AT sequences in DNA with a k_a of $\sim 10^8 \text{ M}^{-1} \text{ s}^{-1}$ that does not vary with the salt concentration as extensively as with the intercalators. The calculated equilibrium constant for the 3,6 carbazole with a k_a of $\sim 10^8 \text{ M}^{-1} \text{ s}^{-1}$ and a k_d of $\sim 150 \text{ s}^{-1}$ at 0.1 M Na⁺ is $>10^6 \text{ M}^{-1}$.

Binding Affinity. To evaluate the relative affinities of the carbazoles for AT DNA sequences (GC polymers have Tms

that are above 95 °C in carbazole complexes), T_m studies were done at saturating ratios of the carbazole to DNA. The 2,7 carbazole complex has a T_m that is $>95^\circ\text{C}$ ($\Delta T_m > 27^\circ\text{C}$) while the 3,6-carbazole has a ΔT_m of 21.6 °C under the same conditions. In the 1:1 complex with the d(CGC-GAATTCGCG)₂ duplex (a longer sequence related to the 10 mer used in NMR experiments) a ΔT_m of 12.0 °C was obtained for the 2,7- and a ΔT_m of 7.8 °C for the 3,6 complex.

Fluorescence spectral changes observed on binding of the 2,7- and 3,6-carbazole compounds to poly[d(A-T)]₂ and poly[d(G-C)]₂ (Figure 2) were used to determine the binding constants from Scatchard plots. Binding measurements were done by titrating DNA samples into solutions of the 2,7 and the 3,6 carbazole compounds at a range of concentrations in MES buffer with 0.1 M NaCl added. The 2,7 carbazole has a binding constant of $1.7 \times 10^7 \text{ M}^{-1}$ on binding to poly[d(A-T)]₂ and $3.4 \times 10^5 \text{ M}^{-1}$ on binding to poly[d(G-C)]₂. On the other hand, the 3,6-carbazole has a lower binding

Table 1: Aromatic Proton Chemical Shifts for Carbazole Compounds Free and Bound to d(A-T)₇ and d(G-C)₇ Oligomers^a


compd	H	d(A-T) ₇			d(G-C) ₇	
		MR = 0 δ	MR = 0.3 δ	$\Delta\delta$	MR = 0.5 δ	$\Delta\delta$
2,7	H1/H8	8.10	7.99	-0.11	7.58	-0.52
	H3/H6	7.70	7.73	+0.03	7.25	-0.45
	H4/H5	8.46	8.48	+0.02	7.85	-0.61
3,6	H1/H8	7.77	7.73	-0.04	7.04	-0.73
	H2/H7	7.90	7.77	-0.13	7.04	-0.86
	H4/H5	8.65	8.50	-0.15	8.01	-0.64

^a R = imidazoline, MR = molar ratio of compound to DNA base pairs. Experiments were conducted in phosphate buffer, pH 7.0 and 0.10 M NaCl. δ at MR = 0, are the chemical shifts for the free compounds at 2×10^{-4} M and $T = 30^\circ\text{C}$.

constant of $6.0 \times 10^6 \text{ M}^{-1}$ on binding to poly[d(A-T)]₂ and a higher binding constant of $7.3 \times 10^5 \text{ M}^{-1}$ with poly[d(G-C)]₂. The preference for AT base pairs of the 2,7-carbazole is greater than for the 3,6-carbazole.

Molecular Modeling. Molecular models of the 2,7- and 3,6-carbazoles were prepared for energy minimization using three initial docking guides: (i) the DNA receptor site was from an X-ray structure of a structurally similar diphenylfuran diamidine (Figure 9) bound into the AATT central site of the duplex d(CGCGAATTCGCG)₂ and the bound diphenylfuran dication was used as a preliminary guide in docking the carbazoles; (ii) the NOE crosspeaks between the AT bases of the DNA and the carbazole aromatic protons specify the carbazole orientation as well as specific contacts in the DNA minor groove; (iii) the diphenylfuran diamidine and other similar minor-groove binding diamidines such as pentamidine and berenil typically make two hydrogen bonds to AN3 and/or TO2 atoms at the floor of the minor groove and it was found that two hydrogen bonds could also be formed with both carbazoles. The NOE contacts and hydrogen bonds were used to refine the docked model, and the complex was energy minimized as described in the Methods Section. A diagram of the hydrogen bonds obtained in the energy-minimized complexes is shown in Figure 9, and the results from X-ray analysis of the diphenylfuran are included for reference. A molecular model of the central region of the 2,7-carbazole-DNA complex is shown in Figure 10 for illustration of the structural features of the fused-ring minor-groove complexes.

With the 2,7 compound strong NOEs to AH2 of the central A of AATT were obtained, and in the energy-minimized model the distance to the carbazole H1 and H8 protons are 2.3 and 2.8 Å from the AH2 of A₁₈ and A₆, respectively (Figure 9), in good agreement with NOE results. Medium to weak NOEs are obtained from the carbazole H1/H8 to TH1' and AH1' of the central A and T of the AATT binding site. In the model these distances are between 3.5 and 4.0 Å, in agreement with NMR results. It is impossible in this orientation for both imidazoline groups of the 2,7-carbazole to form H-bonds with A or T bases at the floor of the groove as the diphenylfuran does, but one imidazoline and the carbazole NH can form very strong H-bonding contacts

(Figure 9): the imidazoline to A₁₈N3 while the carbazole NH forms bifurcated H-bonds to T7 and T19. All hydrogen-bond lengths are between 2.0 and 2.5 Å. The non-H-bonded imidazoline cation is close to the outer edge of the minor groove and can form strong electrostatic interactions with phosphate groups at the edge of the groove (Figure 10). Although the complex is not symmetric, a single set of NMR signals for the carbazole aromatic protons is obtained, and this is also consistent with a dynamic model. The outer imidazoline group can swing into the minor groove while the inner imidazoline swings out so that equivalent complexes can form in a seesaw type manner with the carbazole -NH in essentially the same position in the two complexes.

The 3,6-carbazole was docked into the minor groove as described above for the 2,7 compound. NOE constraints between the 3,6 compound and the minor groove are from the opposite side of the carbazole ring system such that both imidazolines must point into the groove with the carbazole NH pointing out of the groove (Figure 9). In the central AATT binding site of the oligomer duplex the carbazole H4/H5 protons are in close proximity to AH2 protons of A₁₈. The H4/H5 protons are also less than 4 Å from the H1' protons of both T8 and T18 so that the observed NOESY crosspeaks are explained. In this arrangement excellent hydrogen bonds are formed from the carbazole imidazoline groups to TO2 of T8, as in the X-ray structure of diphenylfuran diamidine, and to TO2 of T19 (Figure 9). As can be seen in Figure 9, the furan derivative extends across four base pairs and hydrogen bonds to T8 and T20 while the shorter carbazole extends over only three base pairs. Both hydrogen bonds of the carbazole to TO2 are near the expected value of 2.0 Å. The 3,6-carbazole complex is, thus, much like the "classical" furan diamidine minor-groove complex while the 2,7 carbazole uses only one imidazoline group to contact AT base pairs at the floor of the minor groove.

DISCUSSION

The fused aromatic ring carbazole dications substituted at the 3,6 or 2,7 positions interact with both AT and GC sequences of DNA, but the resulting complexes have dramatically different characteristics with the two sequences. Complexes with similar differences between AT and GC sequences have previously been observed with unfused dications such as DAPI and diphenylfuran derivatives (9, 27, 38, 40). Netropsin, pentamidine, and similar nonplanar dications interact strongly with the minor groove in AT sequences but do not form strong complexes with GC sequences (1, 3-6, 8, 17, 38, 41-46). In spite of significant differences in compound structure, a common mode of minor-groove binding has emerged for complexes of unfused aromatic cations in AT sequences. High-resolution studies of complexes of netropsin (3-6), DAPI (47), berenil (48-50), diphenylfurans (32), and pentamidine (16, 50), for example, illustrate that all of these diverse compounds can fit snugly into the narrow minor groove in AT sequences of DNA and form hydrogen bonds with AN3 and TO2 acceptors at the floor of the groove. The wider groove and amino group of G in the minor groove of GC sequences does not allow similar complexes to form (3-8).

Surprisingly, all results with the fused-ring carbazoles complexed with poly[d(A-T)]₂ or the oligomer d(A-T)₇ are

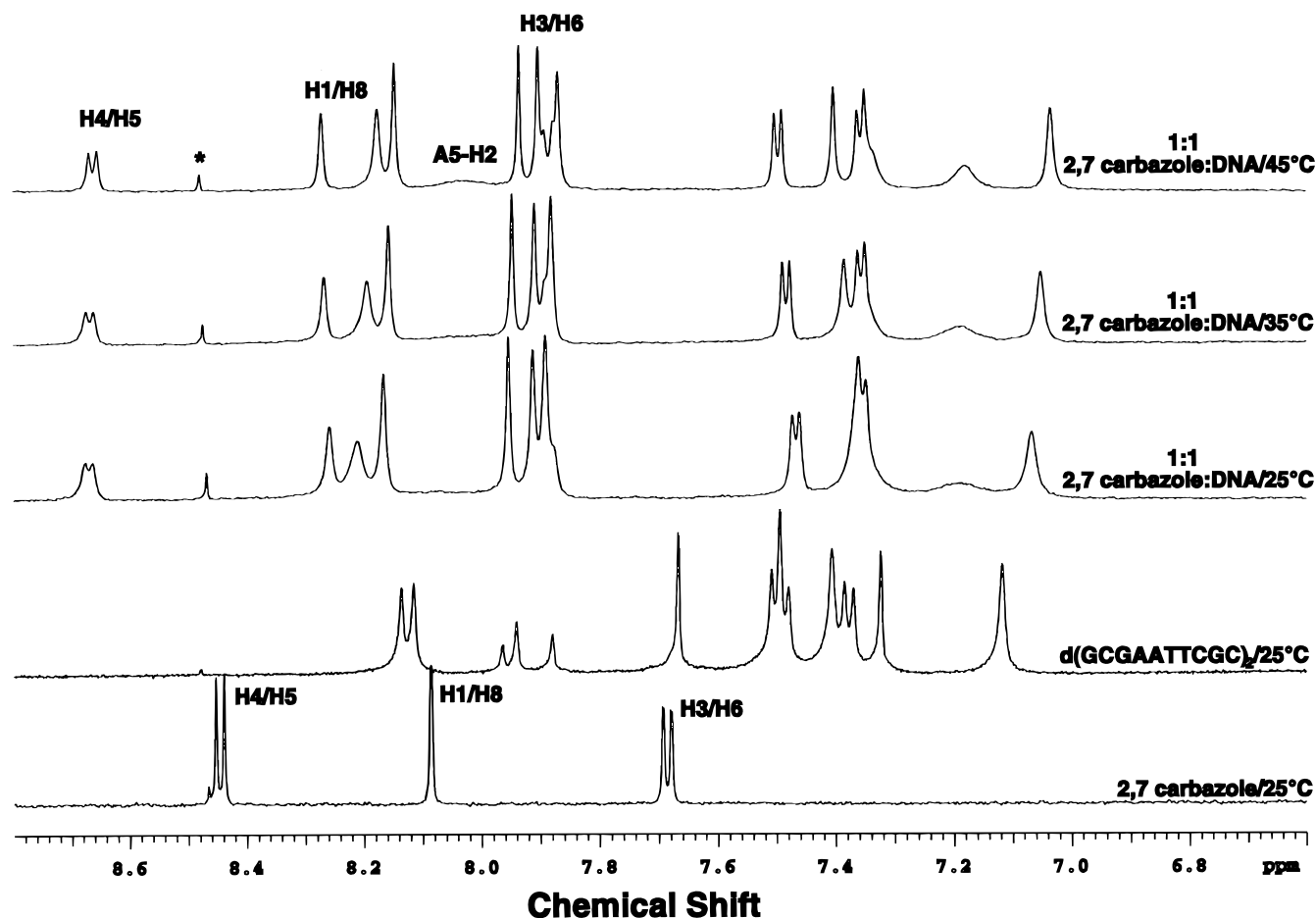


FIGURE 5: 1D Proton NMR spectra of the aromatic region of the 2,7-carbazole complex with $d(GCGAATTCGC)_2$ at different temperatures are shown. The peak labeled with asterisk is impurity from D_2O .

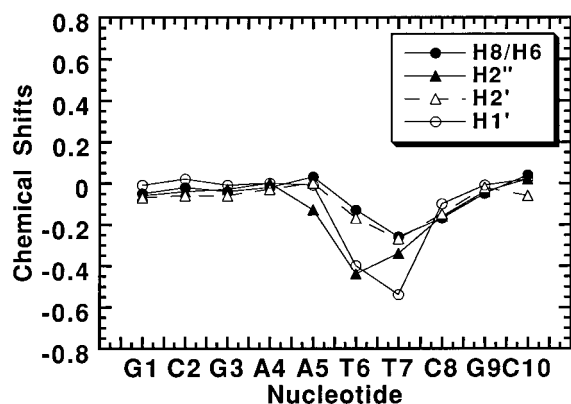


FIGURE 6: Changes in $d(GCGAATTCGC)_2$ chemical shifts on binding the 2,7-carbazole (complex-free) are shown.

in agreement with results expected for minor-groove complex formation: (i) relatively small absorbance changes in the carbazole spectrum on addition of the AT polymer; (ii) large positive induced CD spectral changes in the carbazole region above 300 nm on complex formation; (iii) a slope of ~ 1.8 in a plot of $\log k_d$ versus $-\log(Na^+)$ for dissociation of carbazole-poly[$d(A-T)_2$] complexes; (iv) small, mixed up-field and downfield NMR chemical shifts changes on complex formation; (v) NOEs from carbazole aromatic protons to AH2 and H1' protons in the minor groove. This binding mode for the carbazoles is unexpected for two reasons. First, there are no known fused-ring systems that form strong minor-groove complexes with AT sequences. The carbazole compounds look more like classical intercalat-

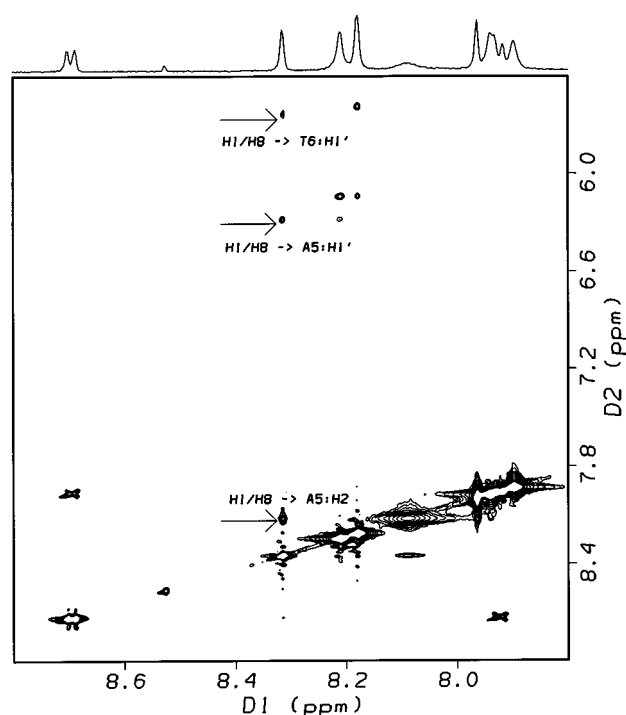


FIGURE 7: Expanded aromatic proton section from the 300 ms NOESY spectrum showing the crosspeaks between H1/H8 of the 2,7-carbazole and $d(GCGAATTCGC)_2$.

ing systems than like the well-known unfused aromatic or peptide compounds that have been identified as AT-specific minor-groove binding agents. Second, in spite of their

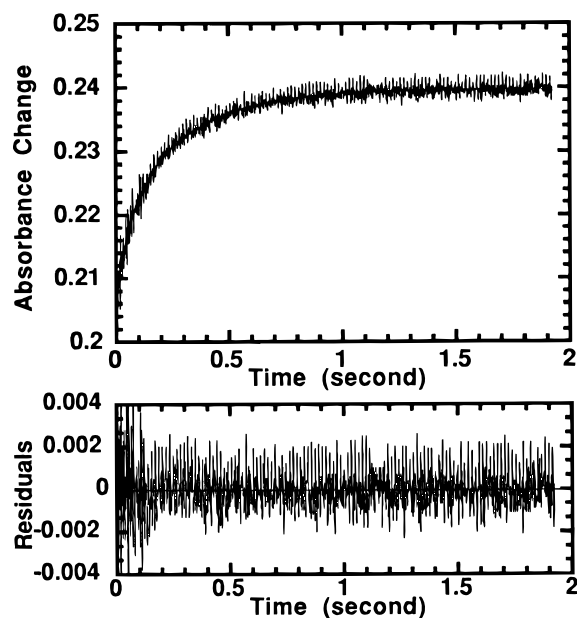


FIGURE 8: Stopped-flow kinetics traces for the SDS-driven dissociation of the 2,7-carbazole from poly[d(A-T)]₂. The experiments were conducted at 20 °C in MES buffer with [Na⁺] = 0.135 M at a ratio of 1:10 compound to polymer base pairs. The concentration of compound **1** after mixing was 1.0×10^{-6} M. The smooth lines in the panels are the two exponential fits to the experimental data. Residual plots are shown under the experimental plot.

different structures and dramatically different radii of curvature (with respect to the two amidines and the carbazole ring system), both compounds form strong complexes in the minor groove at AT base pair sequences. Examination of the experimental results with models for the minor-groove complexes of the carbazoles (Table 1 and Figures 9 and 10) suggests that these compounds represent an important new extension of the results with unfused aromatic groove-binding agents.

A key piece of evidence for development of structural models for the minor-groove complexes comes from NOE results for the carbazole bound to d(GCGAATTCGC)₂ (Figure 7). With the 3,6-carbazole the H4/H5 protons have an NOE crosspeak with an AH2 at the floor of the groove. This requires that H4/H5 point into the minor groove while the carbazole NH points out of the groove; this orients both imidazolines into the groove for hydrogen bond formation (Figure 9). With the 2,7-carbazole the opposite orientation is obtained. Protons H1/H8 of the 2,7 derivatives have an NOE crosspeak to an AH2, indicating that H1/H8 and the carbazole NH point into the groove. In this orientation one imidazoline and the carbazole NH can simultaneously form H-bonds with AN3 and TO2 groups at the floor of the groove while the other imidazoline is close to the lip of the groove and can interact electrostatically with DNA phosphate groups (Figure 9). Weaker NOE crosspeaks to H1' protons in the minor groove are also consistent with these models of minor-groove binding, and the additional interactions help orient the complex structures shown in Figure 10.

With both the 2,7- and 3,6-carbazoles the results on complex formation with GC base pair sequences are completely different from the AT results described and suggest an intercalation binding mode in GC rich sequences with an affinity that is significantly lower than with the AT minor-groove complex. The following results support an intercalation mode at GC sequences: (i) large hypochromic effects

in the carbazole absorption spectrum on GC complex formation; (ii) very small induced CD signals in the carbazole absorption region; (iii) a slope of ~ 0.8 in a $\log k_d$ versus $\log(\text{Na}^+)$ plot for dissociation kinetics; (iv) large (>0.5 ppm) upfield shifts for all carbazole aromatic protons on complex formation with the GC DNAs. The carbazole ring system looks more like classical fused-ring intercalators and the intercalation binding mode at GC sequences is not surprising. An important point of these results, however, is that the affinity of the carbazoles for the AT minor groove is significantly higher than their affinity for GC intercalation sites. Electrostatic interactions and counterion release on complex formation probably provide very similar free energies for complex formation in both AT and GC sequences, and the origin of the AT preference must lie in other interaction components.

Structural studies of a range of minor-groove complexes have demonstrated that van der Waals interactions of the bound ligand as well as hydrogen-bond formation with AN3 and TO2 groups at the floor of the groove provide the primary source of free energy for complex formation. Although strong van der Waals interactions can also be obtained in intercalation complexes, the cost of unwinding the DNA and separating the stacked base pairs to create an intercalation binding site (51) significantly reduces the free energy driving complex formation at intercalation sites. In the oligomer d(GCGAATTCGC)₂, for example, which has both GC intercalation sites and an AT minor-groove site, the only complex detected by NMR experiments at 1:1 ratio of carbazole to duplex is the minor-groove complex.

Models for one way in which the 3,6- and 2,7-imidazoline substituted carbazoles can interact with DNA are shown in Figure 9 and are compared with a similarly substituted diphenylfuran system for which an X-ray structure has been determined in complex with the oligomer duplex d(CGCGAATTCGCG)₂ (32). The furan derivative has a curvature that closely matches that of the DNA minor groove, and it forms cross-strand hydrogen bonds with T bases separated by four base pairs. The 3,6-carbazole is more highly curved with the imidazoline groups closer together than amidines in the furan and it can only span three base pairs. In the model the carbazole forms H-bonds with cross-strand T bases separated by three base pairs. In spite of the fact that two H-bonds are formed in both complexes, the 3,6-carbazole does not form as extensive an array of van der Waals interactions with the DNA groove as the furan and its T_m is significantly less than for the furan (ΔT_m of 8.2 for the carbazole and 11.7 °C for the furan with the oligomer).

The 2,7-carbazole derivative does not have the appropriate curvature to place both cationic groups near the floor of the DNA minor groove to form H-bonds with T- or A-base acceptors, and without the experimental results, it might be assumed that the 2,7-carbazoles would bind weakly to the AT minor-groove receptor site in DNA. As can be seen from the results above, however, this is not observed and the 2,7-carbazole actually binds better to DNA than the 3,6 derivative. Our molecular modeling results have provided evidence for a new type of minor-groove complex for the 2,7 compounds that explains these surprising results (Figure 10). The 2,7-carbazole can form two hydrogen bonds with bases at the floor of the minor groove, as with the furan and the 3,6-carbazole, but the H-bonds are from one imidazoline group and from the carbazole N-H rather than from two

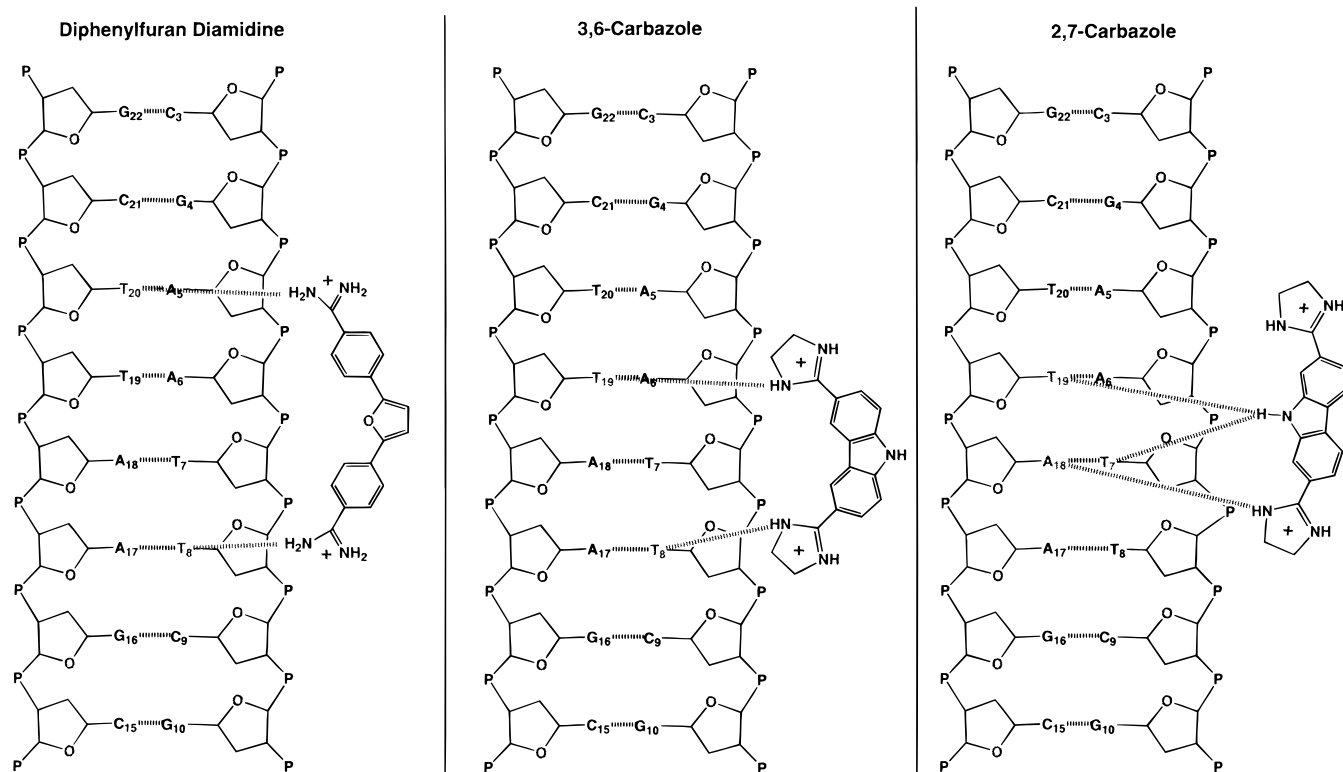


FIGURE 9: Schematic illustrations of the optimized hydrogen bonding of a diphenylfuran diamidine and the two carbazole diimidazolines into the duplex AATT binding site are shown. The furan results are from a crystal structure (Laughton et al., 1996) with the dodecamer duplex $d(\text{CGCGAATTCGCG})_2$ while the carbazole results are from NMR studies reported here with the corresponding decamer duplex $d(\text{GCGAATTCGC})_2$. The numbering system is from the dodecamer to simplify comparisons. The dashed lines from the compounds to the duplex represent optimized hydrogen-bonding interactions formed during constrained molecular modeling.

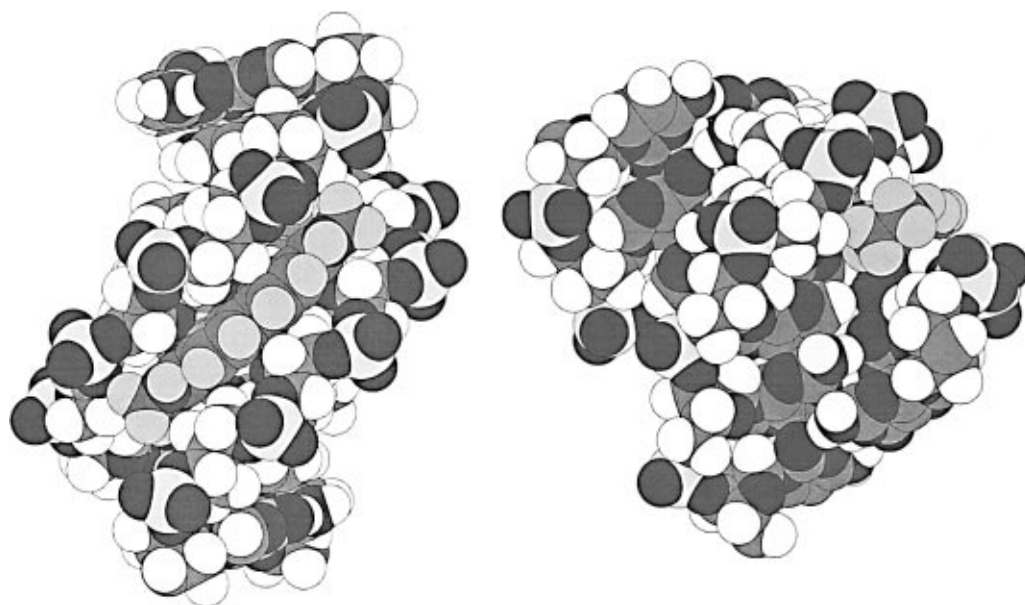


FIGURE 10: Stereoview of the 2,7 carbazole bound to the central $(\text{AATT})_2$ region of the decamer. Only the central region base pairs are shown for clarity: (A, left) view into the minor groove with the carbazole centrally located; (B, right) the model in (A) is rotated back approximately 30° to illustrate the fit of the carbazole into the minor groove. The shading in the models varies from dark to light by atom type as follows: (dark) $\text{O} > \text{N} > \text{C} > \text{P} > \text{H}$ (light). The hydrogen on the carbazole is also shaded gray to help distinguish it from DNA.

imidazoline groups as with the 3,6 compound and with the diphenylfuran (Figure 9). The model indicates that the 2,7 compound has good van der Waals contacts with the DNA minor groove and that additional favorable electrostatic interactions are obtained by the non-H-bonded imidazoline that lies near the outer edge of the minor groove between two DNA phosphate groups (Figures 9 and 10). It should be emphasized that the modeling results of Figures 9 and

10 do not imply that these are the only complex structures possible for the carbazoles bound in the DNA minor groove. The NMR results suggest that the carbazoles can exchange among bound sites and these is probably more than one complex of similar energy in DNA sites of four or more AT base pairs. The point of primary importance, however, which is not model dependent, is that the 3,6- and 2,7-carbazole bind into the minor groove in opposite orientations. NMR

and modeling studies are in progress with additional derivatives to test the proposed model.

SUPPORTING INFORMATION AVAILABLE

2D COSY NMR spectra of 2,7-carbazole with d(A-T)₇ and d(G-C)₇ (Figure S1), aromatic crosspeak region of 300/ms NOESY spectrum of 2,7-carbazole (Figure S2), and plots of log *k*_{app} vs -log[Na⁺] for dissociation of 2,7- and 3,6-carbazole (Figure S3) and association of 3,6-carbazole (Figure S4) (6 pages). Ordering information is given on any current masthead page.

REFERENCES

- Zimmer, C., & Wahnert, U. (1986) *Prog. Biophys. Mol. Biol.* 47, 31–112.
- Coll, M., Frederick, C. A., Wang, A. H.-J., & Rich, A. (1987) *Proc. Natl. Acad. Sci. U.S.A.* 84, 8385–8389.
- Kopka, M. L., & Larsen, T. A. (1992) in *In Nucleic Acid Targeted Drug Design* (Propst, C. L., & Perun, T. J., Eds.) pp 303–374, Marcel Dekker, Inc., New York.
- Kopka, M. L., Pjura, P., Yoon, C., Goodsell, D., & Dickerson, R. E. (1985a) in *Structure and Motion: Membranes, Nucleic Acids and Proteins* (Clementi, E., Corongiu, G., Sarma, M. H., & Sarma, R., Eds.) pp 461, Adenine Press, New York.
- Kopka, M. L., Yoon, C., Goodsell, D., Pjura, P., & Dickerson, R. E. (1985b) *J. Mol. Biol.* 183, 553–563.
- Kopka, M. L., Yoon, C., Goodsell, D., Pjura, P., & Dickerson, R. E. (1985c) *Proc. Natl. Acad. Sci. U.S.A.* 82, 1376–1380.
- Pjura, P. E., Grzeskowiak, K., & Dickerson, R. E. (1987) *J. Mol. Biol.* 197, 257–271.
- Wilson, W. D. (1996) in *Nucleic Acids in Chemistry and Biology* (Blackburn, G. M., & Gait, M. J., Eds.) 2nd ed., Chapter 8, IRL Press.
- Wilson, W. D., Tanious, F. A., Barton, H. J., Jones, R. L., Fox, K., Wydra, R. L., & Strekowski, L. (1990a) *Biochemistry* 29, 8452–8461.
- Wilson, W. D., Tanious, F. A., Buczak, H., Ratmeyer, L., Venkatramanan, M. K., Kumar, A., Boykin, D. W., & Munson, R. (1992) in *Structure and Function, Vol. 1: Nucleic Acids* (Sarma, R. H., & Sarma, M. H., Eds.) pp 83–105, Adenine Press, Schenectady, NY.
- Moskowitz, L., Hensley, G. T., Chan, J. C., & Adams, K. (1985) *Arch. Pathol. Lab. Med.* 109, 735–738.
- Niedt, G. W., & Schinella, R. A. (1985) *Arch. Pathol. Lab. Med.* 109, 727–734.
- Bell, C. A., Cory, M., Fairley, T. A., Hall, J. E., & Tidwell, R. R. (1991) *Antimicrob. Agents Chemother.* 35, 1099–1107.
- Bell, C. A., Dykstra, C. C., Aiman, N. A. I., Cory, M., Fairley, T. A., & Tidwell, R. R. (1993) *Antimicrob. Agents Chemother.* 37, 2668–2673.
- Dykstra, C. C., & Tidwell, R. R. (1991) *J. Protozool.* 38, 78S–81S.
- Edwards, K. J., Jenkins, T. C., & Nedidle, S. (1992) *Biochemistry* 31, 7104–7109.
- Fairley, T. A., Tidwell, R. R., Donkor, I., Naiman, N. A., Ohemeng, K. A., Lombardy, R. J., Bentley, J. A., & Cory, M. (1993) *J. Med. Chem.* 36, 1746–1753.
- Boykin, D. W., Kumar, A., Sychala, J., Zhou, M., Lombardy, R. J., Wilson, W. D., Dykstra, C. C., Jones, S. K., Hall, J. E., Tidwell, R. R., Laughton, C., Nunn, C. M., & Neidle, S. (1995) *J. Med. Chem.* 38, 912–916.
- Tidwell, R. R., Geratz, J. D., Dann, O., Volz, G., & Zeh, D. (1978) *J. Med. Chem.* 21, 613–623.
- Tidwell, R. R., Jones, S. K., Naiman, N. A., Berger, I. C., Brake, W. R., Dykstra, C. C., & Hall, J. E. (1993) *Antimicrob. Agents Chemother.* 37, 1713–1716.
- Patrick, D. A., Boykin, D. W., Tanious, F. A., Wilson, W. D., Bender, B. C., Hall, J. E., Dykstra, C. C., Ohemeng, K. A., & Tidwell, R. R. (in press) *Eur. J. Med. Chem.*
- Wilson, W. D., Wang, Y.-H., Kusuma, S., Chandrasekaran, S., Yang, N. C., & Boykin, D. W. (1985) *J. Am. Chem. Soc.* 107, 4989–4995.
- Fasman, G. D. (1975) in *Nucleic Acids* (Fasman, G. D., Ed.) pp 589, CRC Press, Cleveland, OH.
- Wilson, W. D., & Lopp, I. G. (1979) *Biopolymers* 18, 3025–3041.
- Wilson, W. D., Krishnamoorthy, C. R., Wang, Y.-H., & Smith, J. C. (1985) *Biopolymers* 24, 1941–1961.
- Kibler-Herzog, L., Kell, B., Zon, G., Shinozuka, K., Mizan, S., & Wilson, W. D. (1990) *Nucleic Acids Res.* 18, 3545–3555.
- Wilson, W. D., Tanious, F., Barton, H., Jones, R., Strekowski, L., & Boykin, D. (1989) *J. Am. Chem. Soc.* 111, 5008–5010.
- States, D. J., Haberkorn, R. A., & Ruben, D. J. (1982) *J. Magn. Reson.* 48, 286–292.
- Weiner, S. J., Kollman, P. A., Case, D. A., Singh, U. C., Ghio, C., Alagona, G., Profeta, S., Jr., & Weiner, P. (1984) *J. Am. Chem. Soc.* 106, 765–784.
- Weiner, S. J., Kollman, P. A., Nguyen, D. T., & Case, D. A. (1986) *J. Comput. Chem.* 7, 230–252.
- Veal, J. M., & Wilson, W. D. (1991) *J. Biomol. Struct. Dynam.* 8, 1119–1145.
- Laughton, C. A., Tanious, F. A., Nunn, C. M., Boykin, D. W., Wilson, W. D., & Neidle, S. (1996) *Biochemistry* 35, 5655–5661.
- Wilson, W. D. (1995) in *Encyclopedia of NMR* (Grant, D. M., & Harris, R. K., Eds.) pp 1758–1768, Wiley.
- Hare, D. R., Wemmer, D. E., Chou, S. H., Drobný, G., & Reid, B. R. (1983) *J. Mol. Biol.* 171, 319–336.
- Klevit, R. E., Wemmer, D. E., & Reid, B. R. (1986) *Biochemistry* 25, 3296–3303.
- Lane, A. N., Jenkins, T. C., Brown, T., & Neidle, S. (1991) *Biochemistry* 30, 1372–1385.
- Wilson, W. D., Tanious, F. A., Barton, H. J., Wydra, R. L., Jones, R. L., Boykin, D. W., & Strekowski, L. (1990b) *Anti-Cancer Drug Design* 5, 31–42.
- Wilson, W. D., Tanious, F. A., Buczak, H., Venkatramanan, M. K., Das, B. P., & Boykin, D. W. (1990) in *Molecular Basis of Specificity in Nucleic Acid-Drug Interactions* (Pullman, B., & Jortner, J., Eds.) pp 331–353, Kluwer Academic Publishers, The Netherlands.
- Wilson, W. D., & Tanious, F. A. (1994) in *Molecular Aspects of Anticancer Drug-DNA Interactions* (Neidle, S., & Waring, M., Eds.) pp 243–269, The Macmillan Press Ltd., London.
- Colson, P., Houssier, C., & Bailly, C. (1995) *J. Biomol. Struct. Dynam.* 13, 351–366.
- Lee, M., Rhodes, A. L., Wyatt, M. D., Forrow, S., & Hartley, J. A. (1993a) *Anti-Cancer Drug Design* 8, 173–192.
- Lee, M., Rhodes, A. L., Wyatt, M. D., Forrow, S., & Hartley, J. A. (1993b) *Biochemistry* 32, 4237–4245.
- Lown, J. W. (1989) *Org. Prep. Proc. Int.* 21, 1.
- Lown, J. W. (1990) in *Molecular Basis of Specificity in Nucleic Acid-Drug Interactions* (Pullman, B., & Jortner, J., Eds.) pp 103–122, Kluwer Academic Publishers.
- Lown, J. W., Krowicki, K., Balzarini, J., Newman, R. A., & Clercq, E. D. (1989) *J. Med. Chem.* 32, 2368.
- Lown, J. W., Morgan, A. R., Yen, S.-F., Wang, Y.-H., & Wilson, W. D. (1985) *Biochemistry* 24, 4028.
- Larsen, T. A., Goodsell, D. S., Cascio, D., Grzeskowiak, K., & Dickerson, R. E. (1989) *J. Biomol. Struct. Dynam.* 7, 477–491.
- Brown, D. G., Sanderson, M., Garman, E., & Neidle, S. (1992) *J. Mol. Biol.* 226, 481–490.
- Brown, D. G., Sanderson, M., Skelly, J. V., Jenkins, T. C., Brown, T., Garman, E., Stuart, D. I., & Neidle, S. (1990) *EMBO* 9, 1329–1334.
- Jenkins, T. C., Lane, A. N., Nedidle, S., & Brown, D. G. (1993) *Eur. J. Biochem.* 213, 1175–1184.
- Wilson, W. D. (in press) in *DNA and Aspects of Molecular Biology* (Kool, E., Ed.) Pergamon Press, New York.